Identification of the Autophosphorylation Sites of LRRK2

ARTICLE *in* BIOCHEMISTRY · OCTOBER 2009

Impact Factor: 3.02 · DOI: 10.1021/bi9011379 · Source: PubMed

3 AUTHORS, INCLUDING:

Genta Ito
University of Dundee
17 PUBLICATIONS **613** CITATIONS

SEE PROFILE

BIOCHEMISTRY
including biophysical chemistry & molecular biology
Article

Biochemistry **2009,** *48,* 10963–10975 10963
DOI: 10.1021/bi9011379

Identification of the Autophosphorylation Sites of LRRK2†

Shogo Kamikawaji,‡,# Genta Ito,§,# and Takeshi Iwatsubo*,‡,§

‡*Department of Neuropathology and Neuroscience, Graduate School of Pharmaceutical Sciences, University of Tokyo, 7-3-1 Hongo, Bunkyoku, Tokyo, 113-0033 Japan, and* §*Department of Neuropathology, Graduate School of Medicine, University of Tokyo, 7-3-1 Hongo, Bunkyoku, Tokyo, 113-0033 Japan*#*These authors contributed equally to this work.*

Received July 4, 2009; Revised Manuscript Received September 23, 2009

ABSTRACT: Parkinson's disease (PD) is a major adult-onset neurodegenerative disorder affecting the extrapyramidal motor system. A subset of patients develop PD as an autosomal dominant trait, of which PARK8 caused by mutations in the leucine-rich repeat kinase 2 (LRRK2) gene is highlighted because of its high frequency and clinicopathological similarity to sporadic PD. Previous studies have suggested that overactivation of LRRK2 caused by missense mutations leads to neuronal toxicity in PARK8, although the regulatory mechanism that governs the kinase activity of LRRK2 remains unknown. In this study, we expressed the carboxyl-half fragments of LRRK2 (ΔN-LRRK2) that harbors the kinase as well as the ras-like (ROC) domains in Sf9 cells, subjected them to in vitro phosphorylation reaction, and analyzed the autophosphorylation by matrix assisted laser desorption/ionization- time of flight (MALDI-TOF) mass spectrometer. We identified Ser1403, Thr1404, Thr1410, Thr1491 located within the ROC domain, as well as Thr1967 and Thr1969 in the kinase domain, as the autophosphorylation sites. Substitution of Thr1967, an autophosphorylation site located within the kinase domain, to Ala caused a significant decrease in the kinase activity, implicating Thr1967 in the kinase activity of LRRK2. Phosphospecific antibodies to the autophosphorylation sites specifically recognized full-length LRRK2 subjected to in vitro phosphorylation reaction, indicating that the autophosphorylation takes place in holoproteins. Further analysis of autophosphorylation will clarify the mechanism of activation of LRRK2, as well as the pathomechanism of PD in relation to overactivation of LRRK2.

Parkinson's disease (PD) is one of the most common neurodegenerative disorders of adult-onset presenting extrapyramidal symptoms including rigidity, tremor, and akinesia (*1*). The brains of patients with PD are neuropathologically characterized by loss of dopaminergic neurons in substantia nigra or noradrenergic neurons in the locus ceruleus accompanied by the appearance of Lewy bodies, a hallmark lesion of PD, in the cytoplasm of remaining neurons (*2*−*4*). The majority of patients develop PD in a sporadic fashion, whereas a subset of patients inherit PD as an autosomal dominant or recessive traits (*5*). So far, at least six genes have been identified as responsible genes for familial PD (FPD) (*5*). LRRK2[1] is the causative gene for PARK8, an adult-onset, autosomal-dominant form of FPD (*6*, *7*). Genetic linkage of at least six mutations (R1441C/G/H, Y1699C, G2019S, and I2020T) have been established in PARK8 pedigrees (*8*). In addition, LRRK2 mutations have also been found in sporadic PD cases of some ethnic populations (e.g., Ashkenazi Jewish), leading to the notion that LRRK2 mutations are one of the major genetic factors involved in PD (*9*). PARK8 patients harboring mutations of the LRRK2 gene exhibit clinical manifestations similar to those of typical PD in adulthood; pathologically, pleiomorphic features in nigral degeneration, frequently associated with Lewy bodies and α-synuclein deposits, sometimes presenting with pure nigral degeneration without fibrous protein deposits or with tau-positive inclusions, characterize PARK8 (*10*). Thus, analysis of the pathomechanism whereby mutations in the LRRK2 gene cause neurodegeneration should provide important clues to the pathogenesis of familial as well as sporadic forms of PD.

LRRK2 is a large cytoplasmic protein comprised of 2527 amino acids, consisting of several putative functional domains: leucine-rich repeat (LRR) and WD40 repeat motifs presumably involved in protein−protein interactions, ROC (Ras of complex proteins) domain reminiscent of small GTP-binding proteins, and a protein kinase domain. A family of proteins with a similar set of functional domains have been termed the ROCO protein family, which are phylogenetically conserved from slime molds to mammals (*11*). LRRK2 has been shown to exhibit a protein kinase activity, which is upregulated by some FPD mutations (e.g., G2019S or I2020T) (*12*, *13*). Also, it has been reported that overexpression of FPD mutant LRRK2 induces cell death and the toxic effect of LRRK2 is dependent on its kinase activity (*14*, *15*). Accordingly, it has been hypothesized that an abnormal activation of LRRK2 by genetic mutations or other factors might cause neurodegeneration in PARK8 or some form of sporadic PD. From this viewpoint, elucidation of the mechanism of activation of LRRK2 would provide important clues as to the molecular pathomechanism of neurodegeneration in PD. We have previously shown that LRRK2 exists as a GTP-bound form in cultured cells, and that GTP binding to the ROC domain

†This work was supported by the Ministry of Education, Science, Culture and Sports on Priority Areas-Advanced Brain Science Project and for the Global Center of Excellence Program, by Core Research for Evolutional Science and Technology of JST, Japan, and by the Innovation Program of Elan Pharmaceuticals.

*To whom correspondence should be addressed. Tel: 81-3-5841-3541. Fax: 81-3-5841-3613. E-mail: iwatsubo@m.u-tokyo.ac.jp.

[1]Abbreviations: LRRK2, leucine-rich repeat kinase 2; HEK, human embryonic kidney; ROC, Ras of complex proteins; FL, full-length; PSD, postsource decay.

Published on Web 10/13/2009

is essential to the kinase activity of LRRK2 (*16*). However, little is known about the precise mechanism of activation of LRRK2.

To further elucidate the mechanism of activation of LRRK2, we investigated the autophosphorylation of LRRK2, a characteristic feature of LRRK2 (*12*−*17*), because autophosphorylation has been shown to play a pivotal role in the regulation of kinase activity in a wide variety of protein kinases (*18*−*20*). Here we show that LRRK2 autophosphorylates several residues of its own ROC as well as the kinase domains, and that Thr1967 and Thr1491 play important roles for the regulation of kinase activity of LRRK2.

EXPERIMENTAL PROCEDURES

Construction of Expression Plasmids. The expression plasmid of full-length human LRRK2 cloned in the p3xFLAG-CMV-10 vector (SIGMA) was constructed as described previously (*16*). The DNA fragment corresponding to ΔN-LRRK2 (1326−2527 aa) was amplified by PCR using following oligonucleotides as PCR primers: 5′-CAC CTT AAA AAA GGC TGT G-3′ and 5′-TTA CTC AAC AGA TGT TCG TCT C-3′, and the obtained DNA fragment was first cloned into the pENTR/TEV/D-TOPO vector (Invitrogen) and then transferred to the pDEST27 vector (Invitrogen) by recombination using the LR clonase (Invitrogen). Single-nucleotide substitution was introduced into a fragment less than 1.5 kb in size by a long PCR protocol, and the following oligonucleotides were used as PCR primers: 5′-ATA TAC CGA GCC CTG AAA CCC-3′ for D1994A, 5′-GTG AGG AAT TCT ATG CTA CTC ATC C-3′ for S1403A, 5′-CAT TTT ATG GCA CAG CGA GC-3′ for T1410A, 5′- GAA TGC CGC CGA GGA ATC-3′ for T1491A, 5′-CCG AGG AAG CTG ATG CTT TG-3′ for S1494A, 5′-CAA AGC CGC CCT CAC TAG-3′ for S1965A, 5′-CAG CCT CGC TAG AAC CCT AC-3′ for T1967A, 5′-CCT CAC TAG AGC CCT ACA GCA CAG-3′ for T1969A, 5′-GCC AGC CTC GAT AGA ACC CTG CAG CAC AGG-3′ for T1967D as forward primers and the corresponding complementary sequences as reverse primers. The primers for K1906M and G2019S were described previously (*16*). Mutated fragments were subsequently ligated into the full length of sequence by appropriate digestion and ligation. All constructs generated from PCR products were verified by DNA sequencing. For the baculovirus/Sf9 expression system, ΔN-LRRK2 fragments cloned in the pENTR/TEV/D-TOPO vector were transferred to the pDEST20 vector (Invitrogen). To generate the plasmid encoding GST-Moesin$_{550-564}$, two complementary oligonucleotides (5′-AAT TCC GAC TGG GAC GAG ACA AAT ACA AGA CCC TGC GCC AGA TCC GGC AGG CGC-3′ and 5′- GGC CGC GCC TGC CGG ATC TGG CGC AGG GTC TTG TAT TTG TCT CGT CCC AGT CGG-3′) encoding Moesin$_{550-564}$ were annealed and ligated into *Eco*RI/NotI digested fragment of pGEX-6P-1 (GE Healthcare).

Cell Culture and Transfection. Human embryonic kidney (HEK) 293 cells were maintained in Dulbecco's modified Eagle medium (DMEM; Sigma) supplemented with 10% fetal bovine serum and penicillin/streptomycin (Invitrogen) at 37 °C in 5% CO_2 atmosphere. Transient expression in HEK293 cells was performed by transfecting the plasmids using FuGENE6 (Roche) according to the manufacturer's instructions. Sf9 cells were cultured in Grace's supplemented media (Invitrogen) containing 10% fetal bovine serum, 0.1% Pluronic F-68 (Invitrogen), 100 international units/ml of penicillin, and 100 μg/mL of streptomycin (Invitrogen) in a 1-L spinner flask at 27 °C.

Antibodies and Immunochemical Analysis. A polyclonal antibody raised against the carboxyl-terminus of human LRRK2 (residue 2500−2527) was purchased from Novus Biologicals (NB300−268). Anti-FLAG M2 antibody was purchased from Sigma. Immunoprecipitation of the 3× FLAG-tagged protein was performed as follows: 48 h after transfection, transfected cells were lysed in lysis buffer [50 mM Tris-HCl (pH 7.4), 150 mM NaCl, 0.5% NP-40, 20 mM $MgCl_2$, protease inhibitor cocktail complete EDTA-free (Roche) and phosphatase inhibitor cocktail PhosSTOP (Roche)] for 30 min at 4 °C. Anti-FLAG M2 antibody and Protein G Sepharose 4 Fast Flow (GE Healthcare) were added to the lysate after preclearing with CL4B sepharose (GE Healthcare) in the absence of antibodies, and the mixture was incubated for 2 h at 4 °C. Precipitated immunocomplexes were then washed in the lysis buffer five times and subjected to immunoblot analysis or in vitro analysis. For immunoblot analysis, precipitated proteins were solubilized by boiling in SDS−PAGE sample buffer containing 2% SDS and analyzed by immunoblotting as previously described (*21*). For pull-down of GST-fusion proteins, Glutathione Sepharose 4B (GE Healthcare) was used instead of the anti-FLAG antibody and Protein G Sepharose beads.

Detection of in Vivo Phosphorylation of LRRK2. Detection of in vivo phosphorylation of LRRK2 by metabolic labeling was carried out as described previously (*16*). Briefly, HEK293 cells were cultivated for 48 h after transfection and were metabolically labeled with [^{32}P]orthophosphate (1.85 MBq/dish; PerkinElmer) in phosphate-free DMEM (Invitrogen) for 4 h. The labeled cells were lysed in an ice-cold lysis buffer, and transfected proteins were immunoprecipitated as described above. After an extensive wash, the SDS−PAGE sample buffer was added to immunocomplexes, and samples were boiled for 5 min. Samples were then separated by SDS−PAGE, transferred to a PVDF membrane (Millipore), and subjected to immunoblot analysis. The same membrane was then subjected to autoradiography and analyzed with a BAS-1800 image analyzer (FujiFilm).

Identification of Bound Nucleotides by Thin-Layer Chromatography. Guanine nucleotides bound to the GTP-binding proteins were analyzed as previously described (*16*). Briefly, overexpressed LRRK2 immunoprecipitated from transfected HEK293 cells was metabolically labeled with [^{32}P]orthophosphate. After extensive wash of the immunocomplexes, associated nucleotides were eluted by incubation of the beads in elution buffer (20 mM Tris-HCl pH 7.5, 20 mM EDTA, 2% SDS, 1 mM GTP and 1 mM GDP) at 68 °C for 10 min and then separated by thin-layer chromatography (TLC; Merck) and quantified with a BAS-1800 image analyzer.

In vitro Kinase Assay. In vitro kinase assay was conducted essentially as described previously (*16*). GST-Moesin$_{550-564}$ was used as an exogenous substrate of LRRK2. Briefly, overexpressed LRRK2 was immunoprecipitated as described above, and the resulting immunocomplexes were resuspended in 20 μL of an assay buffer [50 mM Tris-HCl (pH 7.5), 10 mM $MgCl_2$, 2 mM DTT, 0.1 mM EGTA, 100 μM ATP, 3 μg GST-Moesin$_{550-564}$ and 3 μCi of [γ-^{32}P]ATP (PerkinElmer)]. After 15 min incubation at 30 °C, the reaction was stopped by addition of the SDS−PAGE sample buffer and boiling. Samples were separated by SDS−PAGE, transferred to a PVDF membrane, and subjected to immunoblotting. The same membrane was then

subjected to autoradiography and analyzed with BAS-1800 image analyzer.

Purification of ΔN-LRRK2 from Sf9 cells. The competent *Escherichia coli* strain DH10Bac (Invitrogen) was transformed with the pDEST20 vectors harboring wild-type or mutant forms of GST-ΔN-LRRK2, and recombinant baculoviral genomic DNA was purified from DH10Bac. Obtained viral genomic DNA was transfected into Sf9 cells using Cellfectin (Invitrogen) according to the manufacturer's instructions. The culture medium containing recombinant baculoviruses was collected. For the large-scale purification of GST-ΔN-LRRK2, Sf9 cells (1 to 3 × 10^6 cells/mL) were infected with baculovirus and harvested 72 h after infection. Cells were solubilized in a lysis buffer [50 mM Tris-HCl (pH 7.5), 150 mM NaCl, 20 mM $MgCl_2$, 0.5% NP-40, 1 mM sodium orthovanadate, 10% glycerol, protease inhibitor cocktail complete EDTA-free] and the soluble fraction was subjected to affinity purification with Glutathione Sepharose 4B.

In-Gel digestion and MALDI-TOF/MS Analysis of ΔN-LRRK2. Purified GST-ΔN-LRRK2 was subjected to an in vitro phosphorylation reaction and eluted from the beads by adding SDS−PAGE sample buffer. In some cases, ΔN-LRRK2 was released from the beads by TEV protease cleavage. ΔN-LRRK2 separated by SDS−PAGE was briefly stained with Coomassie Brilliant Blue G-250. Excised bands from the gels were reduced with 10 mM dithiothreitol (Nacalai) in 100 mM NH_4HCO_3 (pH 8.0) at 56 °C, for 45 min and alkylated with 55 mM iodoacetamide (Wako) in 100 mM NH_4HCO_3 (pH 8.0) in the dark at room temperature for 30 min. Trypsin solution [20 ng/μL Trypsin Gold mass grade (Promega), 40 mM NH_4HCO_3 (pH 8.0), 10% acetonitrile, 0.1% *n*-octyl-β-D-glucoside (Dojindo)] was added to the gel pieces and incubated at 37 °C for 12−16 h. Digested peptides were collected, dried, and reconstituted in 0.1% TFA. Peptide solutions were then concentrated with ZipTip C_{18} (Millipore) and analyzed by Axima-TOF^2 mass spectrometer (Shimadzu, Japan) using α-cyano-4-hydroxy cinnamic acid (Shimadzu) as a matrix. For phosphopeptide enrichment, Fe^{3+}-IMAC beads were used prior to concentration by ZipTip. To generate Fe^{3+}-IMAC beads, Ni-NTA agarose (Qiagen) was sequentially washed with 100 mM EDTA, water, and 0.1 M acetate and loaded with 100 mM $FeCl_3$ solubilized in 0.1 M acetate. Fe^{3+}-IMAC beads was then washed with water and 0.1 M acetate, and stored in 0.1 M acetate at 4 °C until use. One microliter of digested peptide solutions in 0.1% TFA were incubated with 2 μL of 25% Fe^{3+}-IMAC beads and incubated for 15 min at room temperature. The beads were then sequentially washed three times with 10 μL of 0.1 M acetate and 10 μL of water. For MALDI analysis, 2 μL of 1% phosphoric acid was added to the beads and bound peptides were eluted by incubating the beads for 5 min at room temperature. Eluted peptides were analyzed with a mass spectrometer as described above. Alternatively, the washed Fe^{3+}-IMAC beads were resuspended in a matrix solution and applied directly to the target plate for the sensitive detection. For in situ phosphatase treatment, the peptide samples on the target plate of the mass spectrometer were directly mixed with the phosphatase solution [100 units/mL calf intestine alkaline phosphatase (New England Biolab), 100 mM NH_4HCO_3, pH 8.0], incubated for 5 min at room temperature and analyzed as described above.

Measurement of Michaelis Constant for ATP of ΔN-LRRK2. GST-ΔN-LRRK2 pulled down from overexpressed HEK293 cells was subjected to in vitro phosphorylation in the presence of varying concentrations of [γ-^{32}P]ATP (~1500 cpm/pmol). The initial velocity of reaction was calculated and plotted against a concentration of ATP. Michaelis constant for ATP ($K_{M,ATP}$) was calculated by the double reciprocal Lineweaver−Burk plot.

Generation of Phosphorylation Specific Antibodies. Immunogen phosphopeptide was synthesized by BEX (Tokyo, Japan). Anti-pThr1967 is a rabbit polyclonal antibody raised against amino-terminally KLH (keyhole limpet hemocyanin)-conjugated synthetic phosphopeptide, *C*DKASLpTRTLQH, where pT stands for phosphorylated threonine, amino-terminal cysteine (italic) being added for the conjugation of KLH. Specific recognition of the immunogen peptide was verified by dot blotting: the phosphopeptides were adsorbed onto a nitrocellulose membrane and probed with an antibody according to a standard procedure. For protein phosphatase (λPPase) treatment of LRRK2, immunoprecipitated LRRK2 was resuspended in the λPPase buffer (New England Biolab) and 400 units of λPPase was added to the reaction mixture. The reaction was carried out at 30 °C.

RESULTS

The Carboxyl-Terminal Half Fragment of LRRK2 Undergoes Autophosphorylation in HEK293 Cells. To investigate the functional consequences of autophosphorylation of LRRK2, we first intended to identify the autophosphorylation sites in full-length (FL) LRRK2 (Figure 1A) by mass spectrometry. Besides autophosphorylation, however, FL-LRRK2 is extensively phosphorylated by other kinase(s) in HEK293 cells (Figure 1B) (*16*), which confounds the identification of the autophosphorylated residues in FL-LRRK2. Indeed, MALDI-TOF mass spectrometric analysis of FL-LRRK2 immuno-purified from transfected HEK293 cells revealed clusters of phosphorylated residues around the amino-terminal side of the LRR domain (G.I. and T.I., unpublished observation), consistent with previous reports (*22*). These phosphorylation sites were excluded as autophosphorylation sites because kinase-inactive LRRK2 also was phosphorylated at those residues (*22*) and Ala substitutions of these residues did not affect the kinase activity of LRRK2 (G.I. and T.I., unpublished observations). To eliminate the phosphorylation by other kinase(s) at the amino-terminal region of LRRK2 that occurred in culture cells, we expressed an amino-terminally deleted mutant of LRRK2 lacking the amino-terminal half region including the LRR domain, as an amino-terminally GST-fused protein (GST-ΔN-LRRK2; 1326−2527 aa) (Figure 1A). We confirmed that wild-type (wt) ΔN-LRRK2 retained the kinase activity by in vitro autophosphorylation as well as by in vitro incubation of an exogenous LRRK2 substrate, GST-Moesin$_{500-577}$, whereas the kinase-inactive forms (i.e., K1906M and D1994A) of ΔN-LRRK2 did not, as reported previously (*23*) (Figure 1C and data not shown). We then examined the in vivo phosphorylation of ΔN-LRRK2 by metabolic labeling and found that wt ΔN-LRRK2 underwent phosphorylation in HEK293 cells, whereas the kinase-inactive forms of ΔN-LRRK2 were hardly phosphorylated (Figure 1D). These results strongly suggested that ΔN-LRRK2 is phosphorylated exclusively by its own kinase activity and devoid of phosphorylation by other kinase(s) in HEK293 cells, enabling us to selectively identify the autophosphorylation sites that occur in the carboxyl-terminal region of LRRK2.

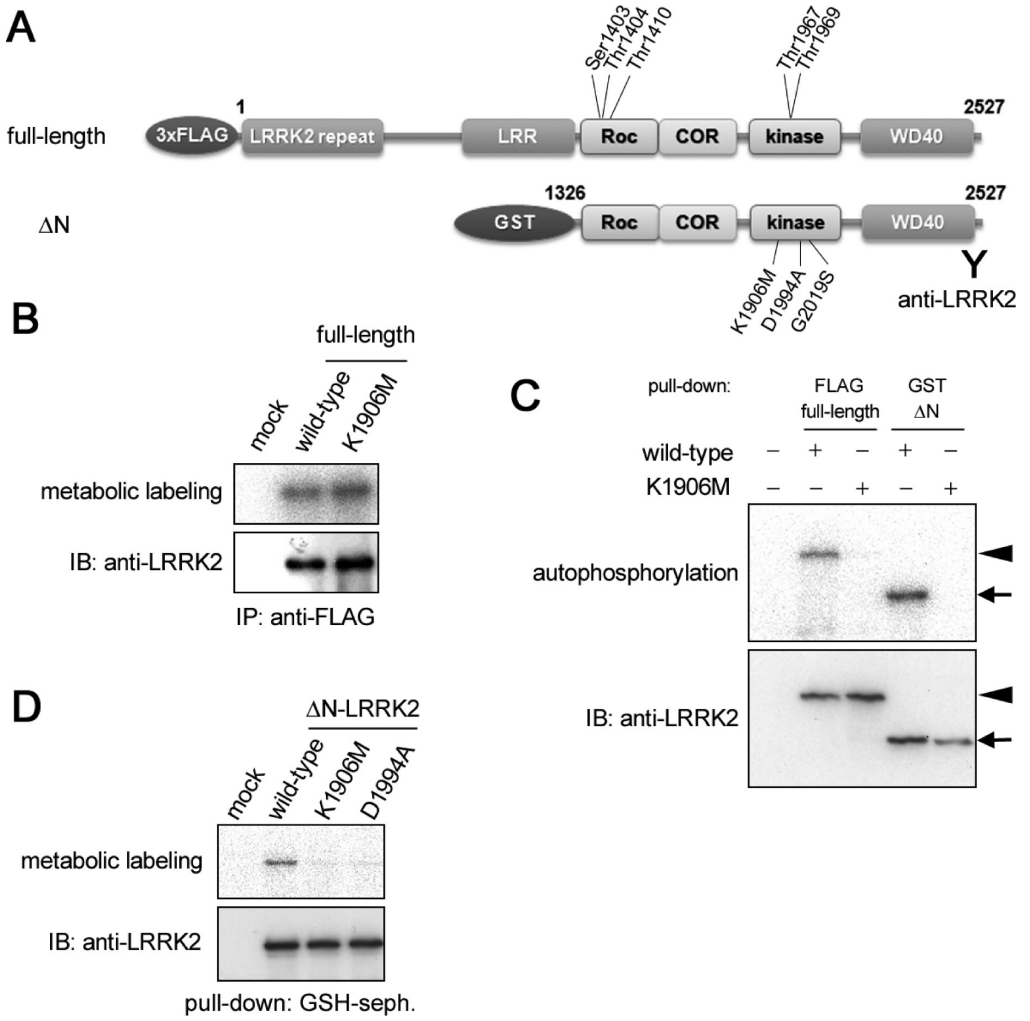

FIGURE 1: (A) Schematic representation of amino-terminally 3× FLAG-tagged full-length (FL) LRRK2 and GST-ΔN-LRRK2. Autophosphorylated residues identified in the present study as well as the mutations used in this study are shown. The epitope of the anti-LRRK2 antibody (2500−2527) used in this study is also shown. (B) Phosphorylation of FL-LRRK2 in HEK293 cells was determined by autoradiography of immunoprecipitated LRRK2 after metabolic labeling of cells with [^{32}P]orthophosphate (top panel). The bottom panel shows immunoblots of immunoprecipitated LRRK2 using anti-LRRK2 to show the equal level of loading. (C) Autophosphorylation activity of ΔN-LRRK2. LRRK2 immunoprecipitated from transfected HEK293 cells were subjected to an in vitro kinase assay. The bottom panel shows immunoblots of immunoprecipitated LRRK2 using anti-LRRK2 to show the equal level of loading. (D) Phosphorylation of ΔN-LRRK2 in HEK293 cells was determined as in (B). Results are representative of at least three independent experiments.

Identification of the Autophosphorylated Peptides Derived from ΔN-LRRK2. To identify the autophosphorylation sites within ΔN-LRRK2, we employed mass spectrometric analyses on ΔN-LRRK2. We first overexpressed wt, K1906M, or G2019S mutant forms of GST-ΔN-LRRK2 in Sf9 cells by baculoviral infection. Overexpressed GST-ΔN-LRRK2 fusion protein was then purified by affinity chromatography using the glutathione-sepharose beads. Purified wt as well as G2019S mutant ΔN-LRRK2 polypeptides were confirmed to retain the autophosphorylation activity (Figure 2A). Since the kinase activity of G2019S mutant was higher than that of wt, we have chosen to further analyze the G2019S mutant for the identification of autophosphorylation sites. G2019S ΔN-LRRK2 autophosphorylated by in vitro phosphorylation reaction was separated by SDS−PAGE and subjected to an in-gel digestion with trypsin. Although amino acid sequences of LRRK2 were easily identified by a peptide mass fingerprinting analysis of the obtained tryptic peptides, peaks corresponding to phosphorylated peptides were not detectable. To further enrich phosphorylated peptides, we employed the immobilized metal-ion affinity chromatography (IMAC) with ferric-ion (Fe^{3+}) as an affinity ligand to the phosphate moiety (Figure 2B) (*24*). After enrichment of phosphopeptides with Fe^{3+}-IMAC, a number of peaks exhibiting the characteristic neutral loss of phosphate (H_3PO_4; −98 Da) or metaphosphate (HPO_3; −80 Da) from a Ser/Thr residue in the postsource decay (PSD) analysis were apparently observed (Figure 2C), ensuring the phosphorylation of the tryptic peptides. Upon analysis of the kinase-inactive K1906M mutant ΔN-LRRK2, these peaks were not detected or significantly smaller than with wt ΔN-LRRK2 (data not shown), suggesting that these peaks were derived by autophosphorylation.

Thr1967 and Thr1969 within the Kinase Domain of ΔN-LRRK2 are Phosphorylated. Among the peak signals, we further analyzed the peaks *a*, *b*, and *c* with a mass/charge (*m*/*z*) number of 1343.41, 1891.16, and 1971.37, respectively, by tandem mass spectrometric analysis (Table 1). The peak *a* (*m*/*z* = 1343.41) was confirmed to be dually phosphorylated because two characteristic peaks corresponding to the neutral loss of one and two phosphate ions, respectively, were observed by PSD analysis (Figure 3A). The *m*/*z* number was consistent

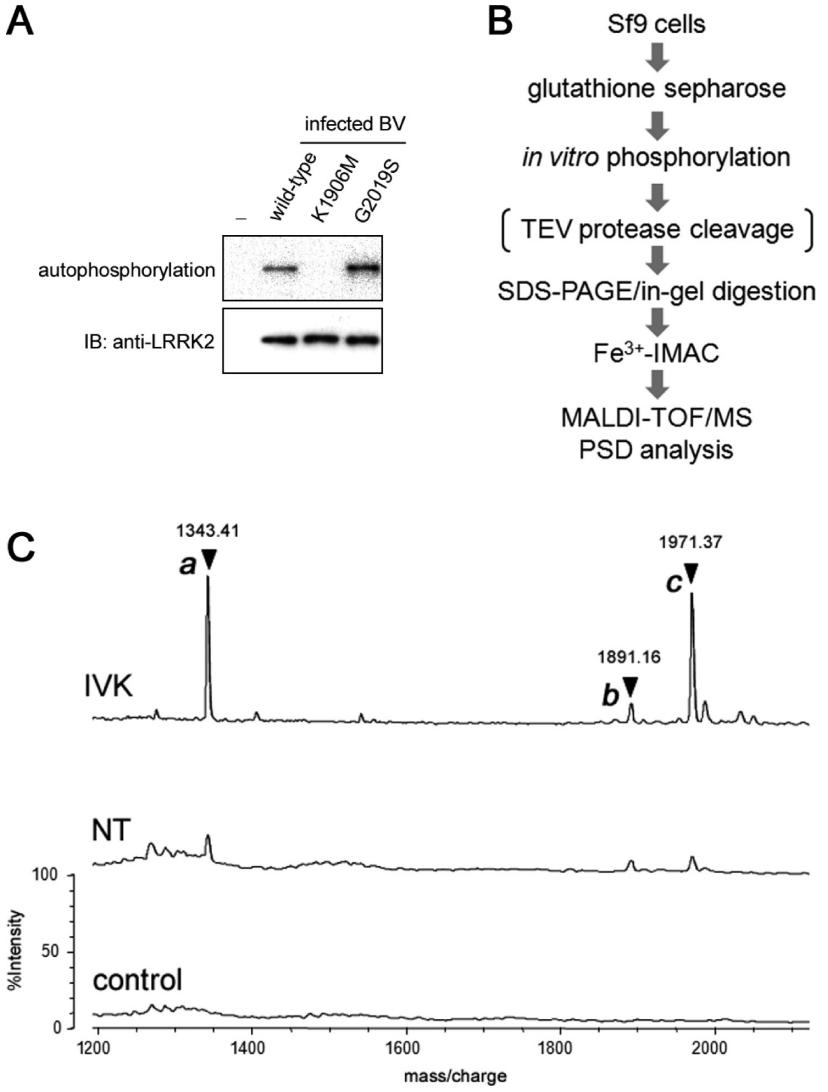

FIGURE 2: (A) The autophosphorylation activity of GST-ΔN-LRRK2 purified from Sf9 cells. Sf9 cells were infected with baculovirus harboring cDNA encoding wild-type, K1906M, or G2019S mutant LRRK2, and overexpressed ΔN-LRRK2 was purified and subjected to an in vitro kinase assay. The bottom panel shows immunoblots of immunoprecipitated LRRK2 using anti-LRRK2 to show the equal level of loading. (B) Schematic depiction of the method for the identification of autophosphorylation sites in ΔN-LRRK2. (C) MALDI-TOF/MS spectra of tryptic peptides derived from G2019S mutant ΔN-LRRK2. Purified ΔN-LRRK2 was subjected to an in vitro kinase (IVK) assay or left untreated (NT) and processed according to the procedure shown in (B). The equivalent position in neighboring empty lane of the gel was processed along with the IVK and NT samples, serving as a negative control (control).

Table 1: The Candidate Peptides Corresponding to the Observed Peaks[a]

			candidate peptides			
peak	observed mass (Da)	number of phosphate	sequence	theoretical mass (Da)	start	end
a	1343.41	2	ASLTRTLQHR	1343.32	1964	1973
b	1891.16	1	DYHFVNATEESDALAK	1890.91	1484	1499
			EEFYSTHPHFMTQR	1890.98	1399	1412
c	1971.37	2	DYHFVNATEESDALAK	1970.89	1484	1499
			EEFYSTHPHFMTQR	1970.96	1399	1412

[a]Amino acid sequences and theoretical average mass numbers of candidate peptides corresponding to peaks *a*, *b*, and *c* in LRRK2 are shown. The number of phosphate was determined by the PSD analysis on each peak. The number of amino acids in FL-LRRK2 corresponding to the *start* and the *end* of candidate peptides are shown.

with that of the peptide ASLTRTLQHR (1964−1973 aa in FL-LRRK2) harboring two phosphates, whose partial amino acid sequence was identified by the shorter fragments generated during the PSD analysis (Table 1, Figure 3A). To further confirm the amino acid sequences of the phosphopeptide, we replaced each one of the Ser/Thr residues (i.e., Ser1965, Thr1967, and Thr1969) in ΔN-LRRK2 with Ala and subjected the mutant protein to the MALDI-TOF/MS analysis after in vitro phosphorylation reaction. The peak *a*′ ($m/z = 1327.19$) derived from S1965A mutant showed a mass number smaller by ~16 Da compared to that of wt ΔN-LRRK2, presumably due to the Ser to Ala substitution (Figure 3B, Table 2a), whereas other peaks

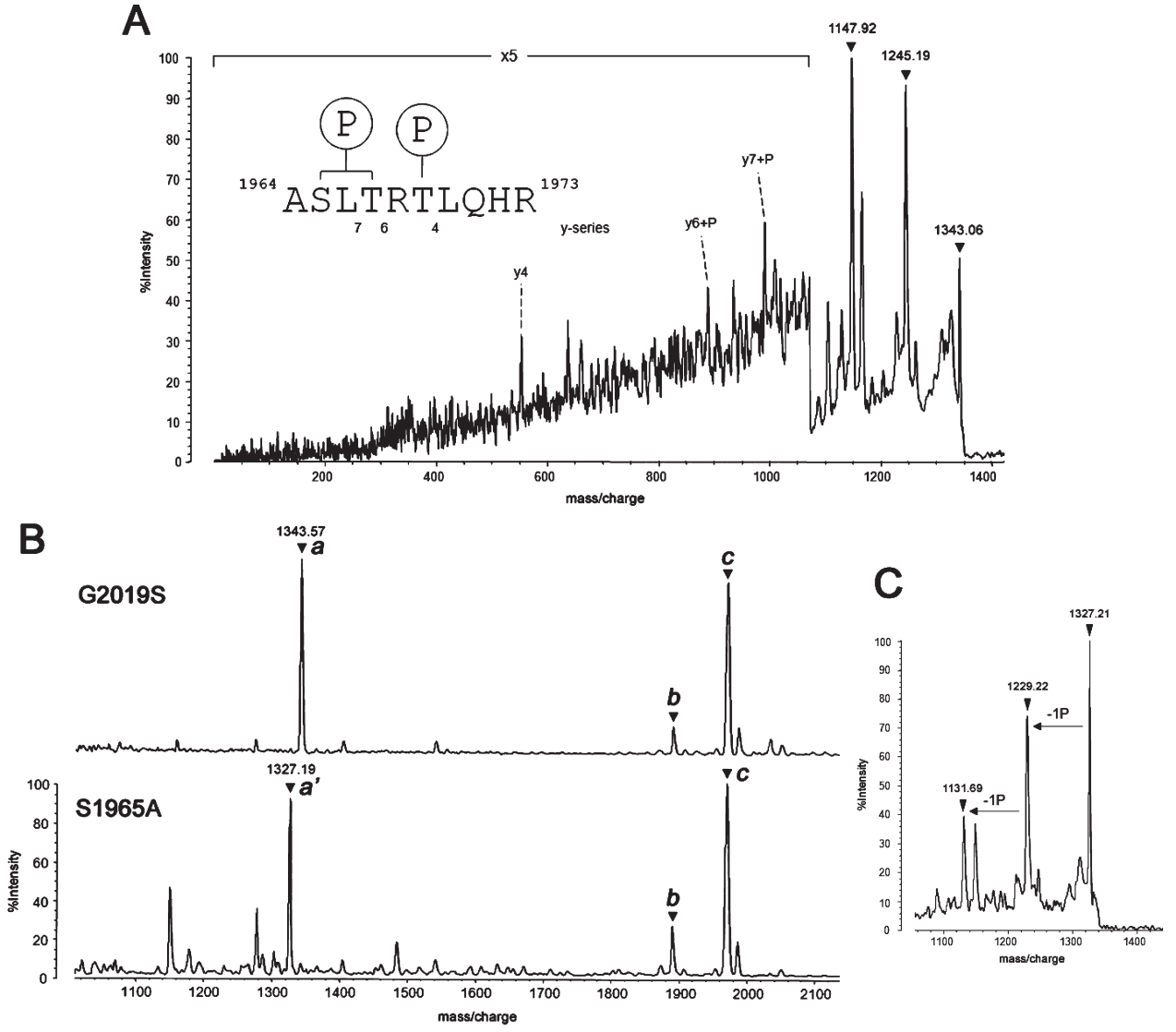

FIGURE 3: (A) PSD spectrum of peak *a*. (B) MALDI-TOF/MS spectra of tryptic peptides derived from G2019S (top) or S1965A (bottom) mutant ΔN-LRRK2. The peaks *a*, *a*′, *b*, and *c* are marked with arrowheads. (C) PSD spectrum of peak *a*′ showing that peak *a*′ contained two phosphates. −1P means the neutral loss of one phosphate (−98 Da).

(*b* and *c*) were not affected. The peak *a*′ (AALTRTLQHR) showed the neutral loss of two phosphate ions (Figure 3C), suggesting that Thr1967 and Thr1969 in the peak *a* (and *a*′) are both phosphorylated. The peak *a* was neither observed in the mass spectra of T1967A nor T1969A mutants, whereas the peaks *b* and *c* were detectable (Figure S1, Supporting Information), further supporting the phosphorylation of Thr1967 and Thr1969 in the peak *a*.

Thr1410 and Thr1491 in the ROC Domain of ΔN-LRRK2 Are Phosphorylated. We next analyzed the peaks *b* and *c* in a manner similar to peak *a*. Peak *b* contained one phosphate ion, whose *m*/*z* numbers were consistent with those of EEFYSTHPHFMTQR (1399−1412 aa) and DYHFVNATEESDALAK (1484−1499 aa) with one phosphate (Table 1). Peak *c* contained two phosphate ions, whose *m*/*z* numbers corresponded to those of the same peptide sequences as peak *b* (Table 1). To further verify the amino acid sequences of peaks *b* and *c*, we digested ΔN-LRRK2 with lysyl endopeptidase, which cleaves the carboxyl-terminus of Lys but not of Arg, and analyzed the phosphorylation sites similarly to the tryptic digests. The peaks with *m*/*z* numbers corresponding to RGFPAIRDYHFVNATEESDALAK (1477−1499 aa) with one and two phosphate ions (theoretical *m*/*z* = 2688.87 and 2768.85, respectively) were observed (Figure 4A). Collectively, we concluded that the peaks *b* and *c* are composed of the peptide DYHFVNATEESDALAK with one and two phosphates, respectively. To substantiate this interpretation, we replaced the two candidate Ser/Thr residues (i.e., Thr1491 and Ser1494) of ΔN-LRRK2 with Ala and examined their phosphorylation states. The S1494A mutant ΔN-LRRK2 yielded peak *b*′ with one phosphate ion (*m*/*z* = 1874.48; peak *b* −16 Da) (Figure 4B, Table 2b), suggesting that the peak *b* consisted of a peptide phosphorylated at Thr1491 (DYHFVNApTEESDALAK). Moreover, treatment of the phosphopeptide-enriched pool fraction obtained from S1494A mutant ΔN-LRRK2 with a calf intestine phosphatase (CIP) on the MALDI target plate yielded a dephosphorylated peptide (*m*/*z* = 1794.73) corresponding to DYHFVNATEEADALAK (Figure 4C), further supporting the view that Thr1491 is phosphorylated. In contrast, the peak *c* derived from S1494A mutant ΔN-LRRK2 showed no shift in the mass spectra (Figure 4B), suggesting that the peak *c* has no relevance to this peptide. Interestingly, peak *b* (*m*/*z* = 1891.60), in addition to peak *b*′, was observed also in the mass spectra of S1494A ΔN-LRRK2 (Figure 4B), suggesting that the original

Table 2: Mass Numbers of Candidate Peptides with Phosphorylation

(a)

		sequence	theoretical mass (Da)[a] +0P	+1P	+2P	observed mass (Da)
peak	*a* (G2019S)	ASLTRTLQHR	1183.36	1263.34	**1343.32**	**1343.57**
	a′ (S1965A)	AALTRTLQHR	1167.37	1247.34	**1327.32**	**1327.19**

(b)

		sequence	theoretical mass (Da)[b] +0P	+1P	+2P	observed mass (Da)
peak	*b* (G2019S)	DYHFVNATEESDALAK	1810.93	**1890.91**	1970.89	**1891.60**
	b′ (S1494A)	DYHFVNATEEADALAK	1794.93	**1874.90**		**1874.48**

(c)

		sequence	theoretical mass (Da)[c] +0P	+1P	+2P	observed mass (Da)
peak	*b* (G2019S)	EEFYSTHPHFMTQR	1811.00	**1890.98**	1970.96	**1891.61**
	b″ (S1403A)	EEFYATHPHFMTQR	1795.00	**1874.98**	1954.96	**1874.87**
	b‴ (T1410A)	EEFYSTHPHFMAQR	1780.97	**1860.95**	1940.93	**1861.64**
peak	*c* (G2019S)	EEFYSTHPHFMTQR	1811.00	1890.98	**1970.96**	**1971.37**
	c″ (S1403A)	EEFYATHPHFMTQR	1795.00	1874.98	**1954.96**	**1954.80**
	c‴ (T1410A)	EEFYSTHPHFMAQR	1780.97	1860.95	**1940.93**	**1941.49**

[a]Theoretical average mass numbers of the peptides derived from G2019S and S1965A with no (+0P), one (+1P), or two (+2P) phosphate(s) are shown. The mass numbers corresponding to the observed mass numbers of the peaks *a* and *a′* in Figure 3B are shown in bold. [b]Theoretical average mass numbers of the peptides derived from G2019S and S1494A with no (+0P), one (+1P), or two (+2P) phosphate(s) are shown. The mass numbers corresponding to the observed mass numbers of the peaks *b* and *b′* in Figure 4B are shown in bold. [c]Theoretical average mass numbers of the peptides derived from G2019S, S1403A, and T1410A with no (+0P), one (+1P), or two (+2P) phosphate(s) are shown. The mass numbers corresponding to the observed mass of the peaks *b*, *b″*, *b‴*, *c*, *c″* and *c‴* in Figure 5A are shown in bold.

peak *b* contained an additional monophosphorylated peptide besides the Thr1491-phosphorylated peptide. To determine whether peak *b* contains signals derived from another candidate peptide EEFYSTHPHFMTQR (1399−1412 aa) harboring one phosphate, we examined the phosphorylation state of S1403A and T1410A mutant forms of ΔN-LRRK2. Peak *b″* (m/z = 1874.87) and peak *b‴* (m/z = 1861.64), showing the expected shift of the m/z number due to Ser/Thr to Ala substitution, were observed in the mass spectra of S1403A and T1410A mutant ΔN-LRRK2, respectively (Figure 5A, Table 2c). Moreover, the partial amino acid sequence corresponding to EEFYSTHPHFMAQR was confirmed upon PSD analysis of the T1410A mutant ΔN-LRRK2 after CIP treatment (Figure 5B). In addition, peak *c* showed a corresponding shift of the m/z numbers, yielding peak *c″* (m/z = 1954.80) and *c‴* (m/z = 1941.49) (Figure 5A, Table 2c), indicating that peak *c* consists of the dually phosphorylated EEFYSTHPHFMTQR. Both peak *c″* (from S1403A mutant) and *c‴* (from T1410A mutant) showed the neutral loss of two phosphate ions, raising the possibility that all of the three Ser/Thr residues (i.e., Ser1403, Thr1404, and Thr1410) could be concomitantly phosphorylated.

Effects of Mutations at the Autophosphorylation Sites within the ROC and Kinase Domains on Kinase Activity. To further clarify the functional consequences of the autophosphorylation of LRRK2, we examined the kinase activity of the Ala mutant forms of LRRK2 substituted at the autophosphorylation sites. We overexpressed wt or Ala mutant FL- and ΔN-LRRK2 in HEK293 cells and examined their kinase activities by autophosphorylation as well as by an in vitro kinase assay using GST-Moesin$_{550-564}$ as an exogenous substrate. When we substituted the autophosphorylation sites located in the ROC domain, neither T1410A nor T1491A substitution affected the kinase activity of FL-LRRK2 (Figure 6A). Although the autophosphorylation activity was slightly increased in T1491A mutant, the kinase activity on an exogenous substrate (i.e., GST-Moesin$_{550-564}$) was not altered (Figure 6A). We also replaced Thr1410 or Thr1491 in FL-LRRK2 with Asp, aiming at mimicking the phosphorylated status of the amino acid residues, and examined their kinase activities. T1491D mutant FL-LRRK2 showed a significantly decreased autophosphorylation as well as the moesin-phosphorylation activities compared to those with wt LRRK2, whereas T1410D mutant showed a comparable kinase activity on GST-Moesin$_{550-564}$ and an increased autophosphorylation activity (Figure 6A). We next investigated whether these mutations alter the GTP binding status of FL-LRRK2. Transfected HEK293 cells were metabolically labeled with [^{32}P]orthophosphate, and bound nucleotides were eluted from the immunoprecipitated FL-LRRK2. T1491D mutant FL-LRRK2 bound less GTP in HEK293 cells compared to wt or other mutant LRRK2 (Figure 6B), suggesting that the autophosphorylation on Thr1491 causes a reduction in GTP-bound form of LRRK2.

We next substituted the autophosphorylation sites in the kinase domain. T1967A mutant LRRK2 showed a significantly decreased autophosphorylation as well as the moesin-phosphorylation activities compared to those with wt LRRK2, whereas T1969A mutation had little effect on the kinase activities

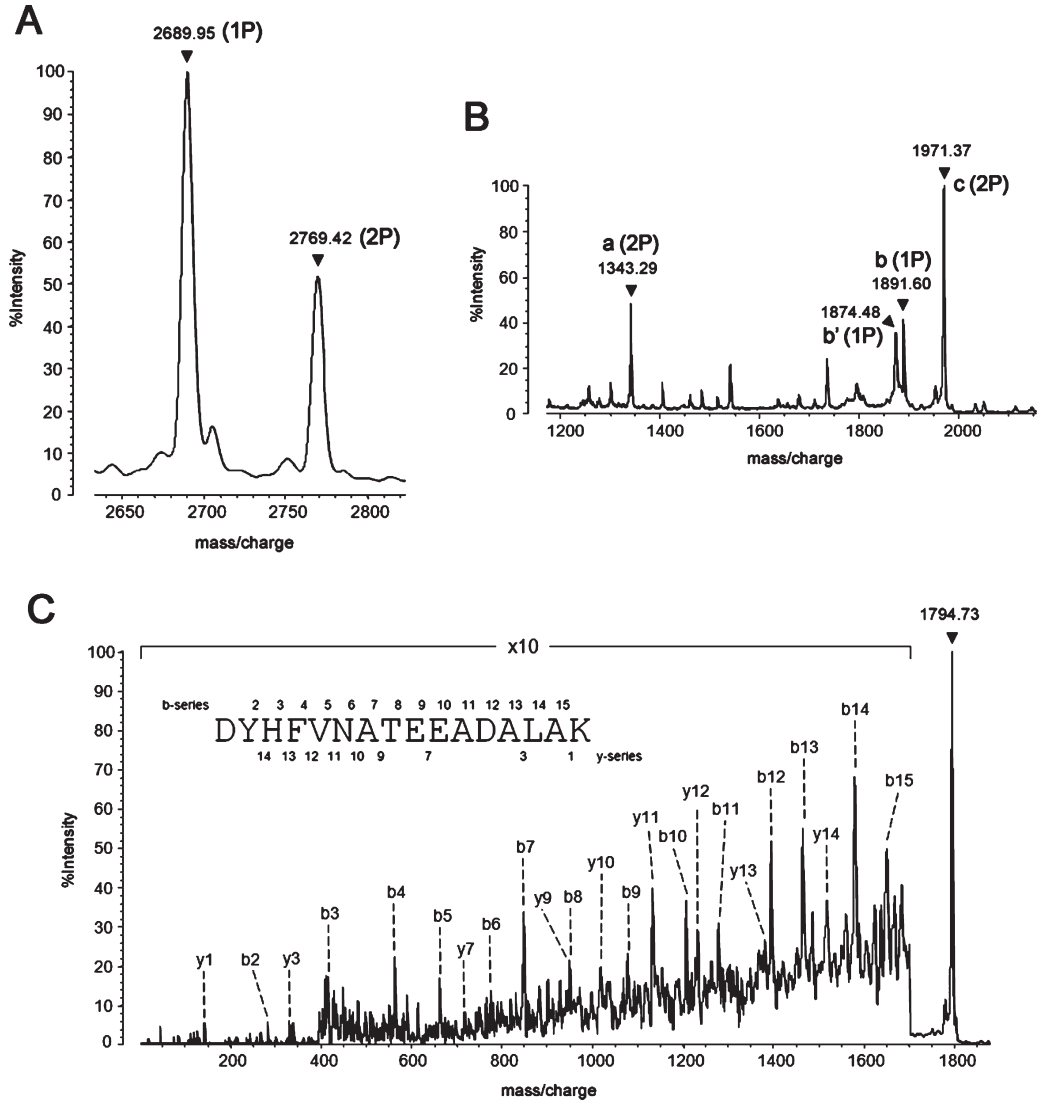

FIGURE 4: (A) MALDI-TOF/MS spectrum of peptides generated by digestion of G2019S mutant ΔN-LRRK2 with lysyl endopeptidase. (B) MALDI-TOF/MS spectrum of tryptic peptides derived from S1494A/G2019S mutant ΔN-LRRK2. Peaks *a*, *b*, *b*′, and *c* were marked with arrowheads. (C) PSD spectrum of the peak *b*′ after dephosphorylation. 1P and 2P mean that the peaks marked with arrowheads contained one and two phosphate, respectively.

(Figure 7A,B). To examine if the kinase domain of T1967A mutant ΔN-LRRK2 is folded in a proper conformation, we calculated the Michaelis constant for ATP ($K_{M,ATP}$) of wt and T1967A mutant ΔN-LRRK2, and confirmed that T1967A mutant ΔN-LRRK2 retained a similar affinity to ATP ($K_{M,ATP}$ = 16.6 ± 2.4 μM; Figure S2, Supporting Information) compared to that of wt ($K_{M,ATP}$ = 20.9 ± 2.8 μM; Figure S2, Supporting Information). We also replaced Thr1967 and Thr1969 in ΔN- and FL-LRRK2 with Asp, aiming at mimicking the phosphorylated status of the amino acid residues, and examined their kinase activities. In contrast to the T1967A mutant, T1967D mutant ΔN-LRRK2 retained comparable kinase activity to that of wt (Figure 7C), whereas T1967D mutant FL-LRRK2 showed a decreased kinase activity (Figure 7D). These results suggested that Thr1967, and possibly its phosphorylation, is important for the kinase activity of LRRK2.

Phosphospecific Antibodies Reveal the Occurrence of LRRK2 Autophosphorylation on a Holoprotein Basis. Because we have analyzed the autophosphorylation sites of LRRK2 on ΔN-LRRK2, we asked whether FL-LRRK2 also is autophosphorylated at the same set of residues. We generated a polyclonal antibody against a synthetic peptide phosphorylated at Thr1967 of LRRK2 (anti-pThr1967; Figure 8A), which specifically recognized the immunogen phosphopeptide by dot blot analysis (Figure 8A). First, we overexpressed ΔN-LRRK2 in HEK293 cells and subjected the immunoisolated ΔN-LRRK2 to an in vitro phosphorylation reaction. Immunoblot analysis revealed that wt, but not K1906M mutant, ΔN-LRRK2 was recognized by the anti-pThr1967 antibody (Figure 8B). Overexpression of FL-LRRK2 gave similar results, suggesting the autophosphorylation of FL-LRRK2 (Figure 8C,D). The anti-pThr1967 antibody labeled G2019S familial Parkinson mutant LRRK2 more intensely than wt LRRK2 (Figure 8C,D), consistent with the abnormal hyperactivity of G2019S mutant LRRK2 (*12*). The reactivity of the anti-pThr1967 was diminished by T1967A substitution, ensuring the specificity of this antibody (Figure 8E,F). Treatment of FL-LRRK2 with λPPase significantly decreased the reactivity of the anti-pThr1967 antibody (Figure 8G), confirming the phosphorylation-dependent reaction of the antibodies to the phosphorylated form of LRRK2.

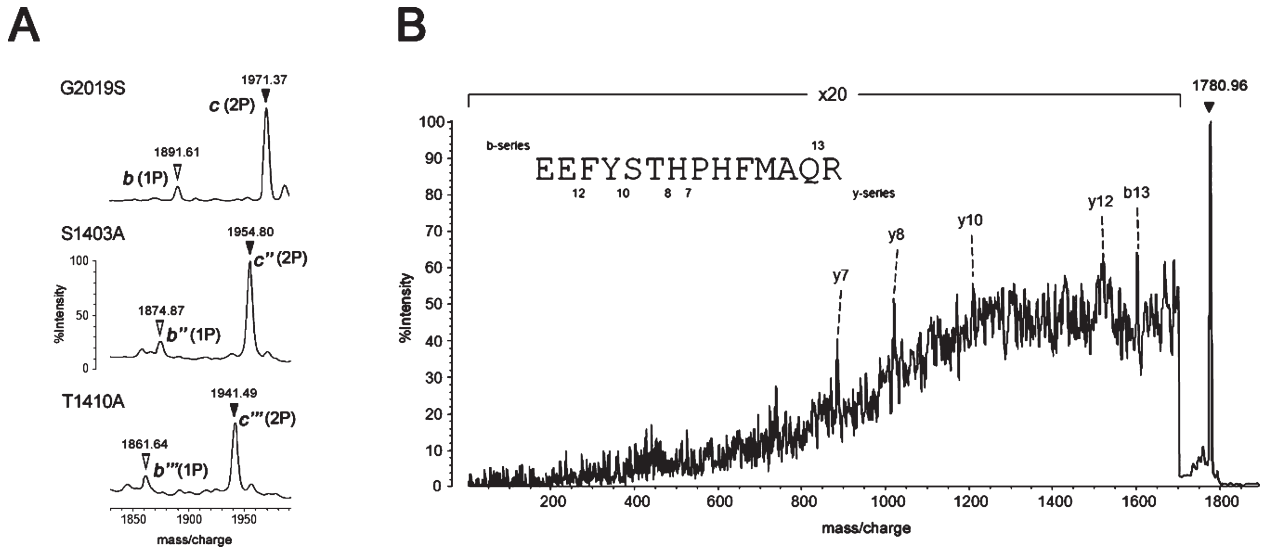

FIGURE 5: (A) MALDI-TOF/MS spectrum of tryptic peptides derived from G2019S, S1403A/G2019S or T1410A/G2019S mutant ΔN-LRRK2. Peaks b, b'', b''', c, c'', and c''' were marked with arrowheads. 1P and 2P mean that the peaks marked with arrowheads contained one and two phosphate(s), respectively. (B) PSD spectrum of the peak b''' after dephosphorylation.

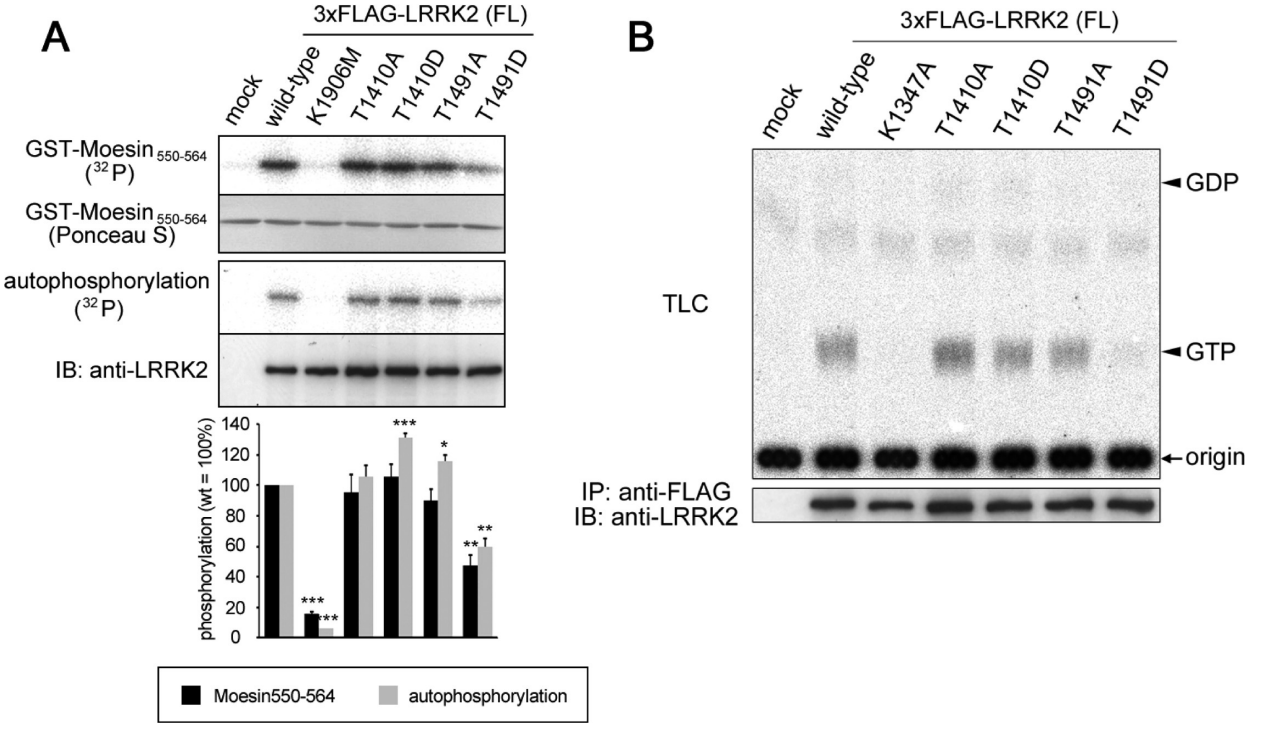

FIGURE 6: (A) The kinase activity of T1410A, T1410D, T1491A, and T1491D mutant FL-LRRK2. LRRK2 immunoprecipitated from transfected HEK293 cells were subjected to an in vitro kinase assay. The kinase activity for GST-Moesin$_{550-564}$ (top panel) as well as the autophosphorylation activity (third panel from the top) were examined. The second panel from the top shows membranes stained with Ponceau S to show the equal level of loading of GST-Moesin$_{550-564}$. The bottom panel shows immunoblots of pulled down LRRK2 using anti-LRRK2 to show the equal level of loading of LRRK2. The levels of the phosphorylation of GST-Moesin$_{550-564}$ (black) as well as autophosphorylation (gray) was quantified and normalized by the expression level determined by immunoblotting. The data are given as the percentage of those observed in wild-type ($n = 3$, mean ± standard error). $^*p < 0.05$, $^{**}p < 0.005$, $^{***}p < 0.001$ (vs wild-type by t-test) (B) The GTP binding activity of T1410A, T1410D, T1491A, and T1491D mutant FL-LRRK2. Bound nucleotides were examined with a thin-layer chromatographic (TLC) analysis. The bottom panel shows immunoblots of pulled down LRRK2 using anti-LRRK2 to show the equal level of loading of LRRK2.

DISCUSSION

A number of protein kinases harbor autophosphorylation activity besides the kinase activity toward exogenous substrates, and the kinase activity is often regulated by autophosphorylation (*18*−*20*). In the present study, we analyzed the autophosphorylation of LRRK2, a protein kinase mutated in a form of autosomal-dominantly inherited PD (PARK8) and found that (i) LRRK2 is autophosphorylated at Ser1403, Thr1404, Thr1410, Thr1491, Thr1967, and Thr1969 in vitro and that (ii) substitution of Thr1491 with aspartate causes a significant decrease in the kinase activity of LRRK2 and that (iii) substitution of Thr1967 with alanine causes a significant decrease in the kinase activity of LRRK2. We have also generated an antibody that recognizes the autophosphorylated form of LRRK2, which

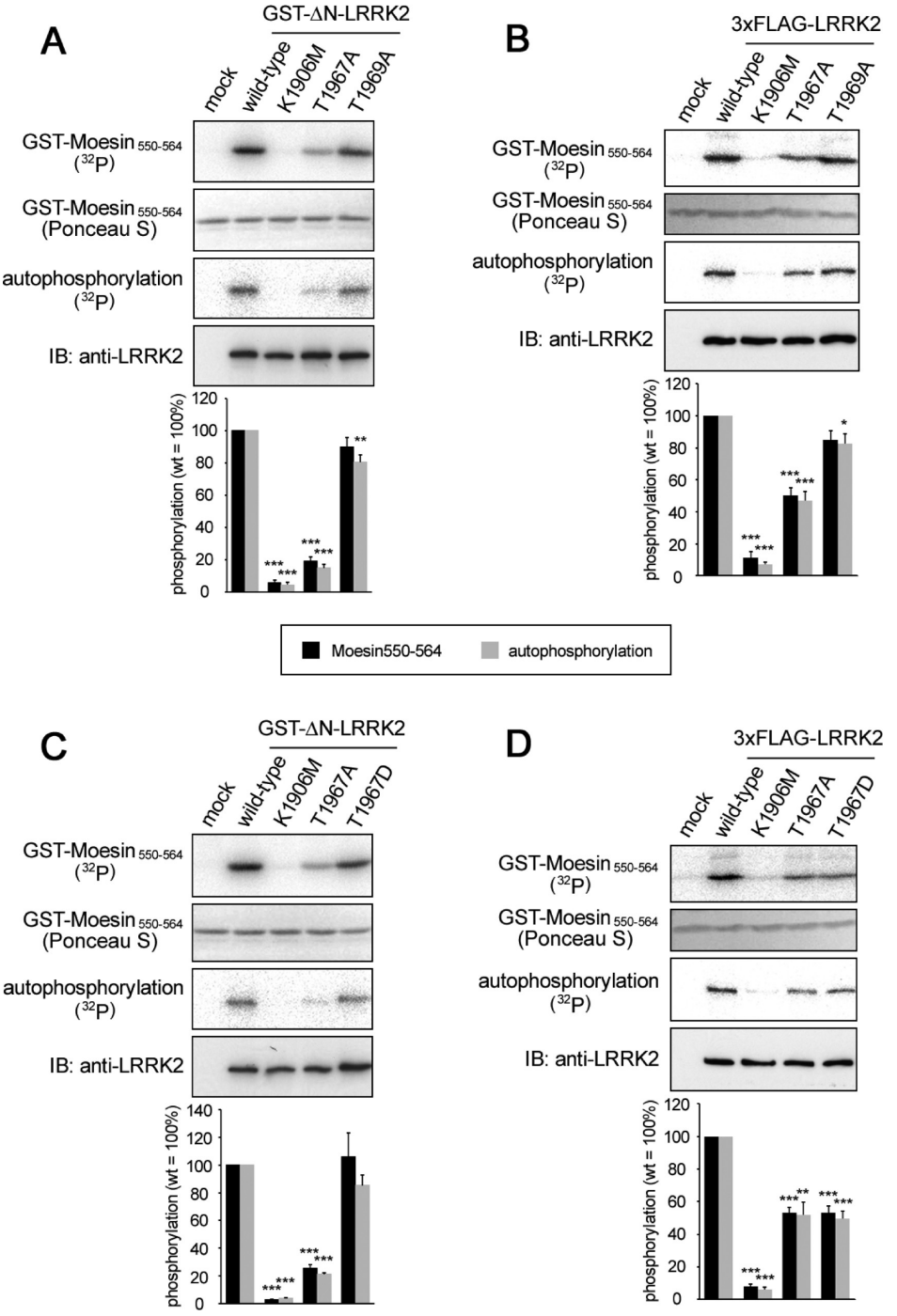

FIGURE 7: (A) The kinase activity of T1967A and T1969A mutant ΔN-LRRK2. LRRK2 pulled down from transfected HEK293 cells were subjected to an in vitro kinase assay. The kinase activities for GST-Moesin$_{550-564}$ (top panel) as well as the autophosphorylation activity (third panel from the top) were examined. The second panel from the top shows membranes stained with Ponceau S to show the equal level of loading of GST-Moesin$_{550-564}$. The bottom panel shows immunoblots of pulled down LRRK2 using anti-LRRK2 to show the equal level of loading of LRRK2. The levels of the phosphorylation of GST-Moesin$_{550-564}$ (black) as well as autophosphorylation (gray) was quantified and normalized by the expression level determined by immunoblotting. (B) The kinase activities of T1967A and T1969A mutant FL-LRRK2 determined as in (A). (C) The kinase activities of T1967A and T1967D mutant ΔN-LRRK2 determined as in (A). (D) The kinase activities of T1967A and T1967D mutant FL-LRRK2 determined as described in (A). The data are given as the percentage of those observed in wild-type ($n = 4$, mean ± standard error). *$p < 0.05$, **$p < 0.005$, ***$p < 0.001$ (vs wild-type by t-test).

enabled us to immunochemically detect the kinase-active form of LRRK2.

We have previously shown that FL-LRRK2 is extensively phosphorylated by other kinases in cultured cells, and that autophosphorylation is assumed to account for a proportion of phosphorylation that occurs on LRRK2 within cells (Figure 1B) (*16*). Therefore, FL-LRRK2 was presumed to be unsuitable for the identification of the autophosphorylation sites in LRRK2. Interestingly, we found that the kinase-inactive form (i.e., K1906M and D1994A) of ΔN-LRRK2, that lacks the N-terminal half of LRRK2 including the LRR domain, fails to undergo phosphorylation within cells, whereas wt ΔN-LRRK2 is phosphorylated (Figure 1D), suggesting that ΔN-LRRK2 escapes from phosphorylation by other kinases in cultured cells

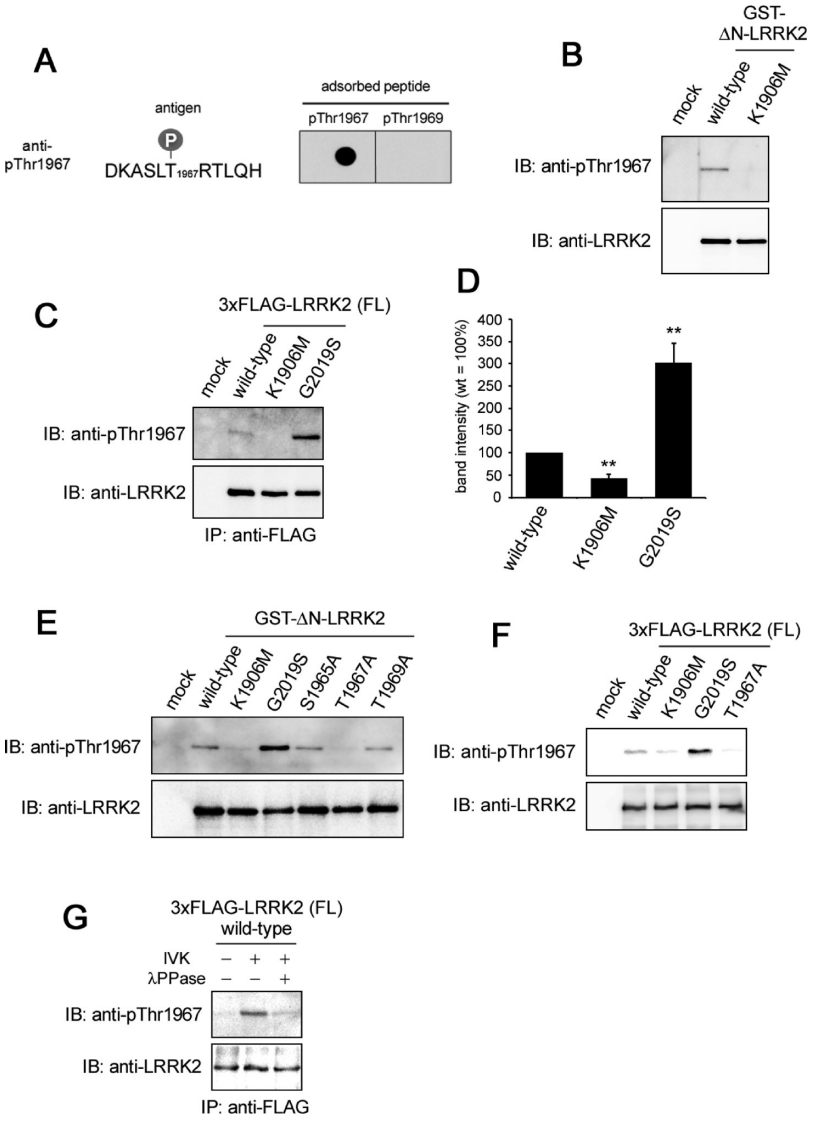

FIGURE 8: (A) Characterization of the anti-pThr1967 phosphorylation-specific antibody. The immunogen phosphopeptide was adsorbed onto nitrocellulose membrane and probed with anti-pThr1967. (B) Wild-type or K1906M mutant ΔN-LRRK2 pulled down from transfected HEK293 cells were subjected to an in vitro kinase assay. ΔN-LRRK2 was subjected to immunoblotting with anti-pThr1967. The bottom panel shows immunoblots of pulled down LRRK2 using anti-LRRK2 to show the equal level of loading. (C, D) Wild-type, K1906M, or G2019S mutant FL-LRRK2 immunoprecipitated from transfected HEK293 cells were subjected to an in vitro kinase assay. FL-LRRK2 was subjected to immunoblotting with anti-pThr1967 (C, top panel). The bottom panels show immunoblots of immunoprecipitated LRRK2 using anti-LRRK2 to show the equal level of loading of LRRK2. The band intensity of phosphorylated FL-LRRK2 probed by anti-pThr1967 was quantified and normalized by the expression level of total FL-LRRK2 as determined by immunoblotting by anti-LRRK2 antibody (D). The data are given as the percentages of that in wild-type LRRK2 ($n = 4-5$, mean ± standard error). **$p < 0.005$ (vs wild-type by t-test) (E, F) T1967A mutant ΔN- (E) and FL- (F) LRRK2 were analyzed by immunoblotting with anti-pThr1967 (G) Wild-type FL-LRRK2 immunoprecipitated from transfected HEK293 cells were subjected to an in vitro kinase assay and/or an in vitro dephosphorylation reaction as indicated above the panel. The bottom panel shows immunoblots of immunoprecipitated LRRK2 using anti-LRRK2 to show the equal level of loading.

and thus might be useful for the identification of autophosphorylated residues in LRRK2. By mass spectrometric analysis using purified and in vitro phosphorylated ΔN-LRRK2, we identified several phosphorylated peptides whose mass numbers are consistent with those derived from ΔN-LRRK2.

To clarify the functional consequences of autophosphorylation, it is crucial to know whether the autophosphorylation of LRRK2 occurs under physiological conditions. Using ΔN-LRRK2, we provided the first evidence that LRRK2 possesses the autophosphorylation activity in cultured cells (Figure 1D). Notably, as shown in Figure 2C, peaks *a*, *b*, and *c* were observed in nontreated samples (NT) as well as those undergoing in vitro kinase (phosphorylation) assay (IVK), suggesting that autophosphorylation identified in this study occurs endogenously and could be amplified by in vitro phosphorylation. We further identified the autophosphorylated residues by tandem mass spectrometric analysis and found that Ser1403, Thr1404, Thr1410, and Thr1491 in the ROC domain, and Thr1967 and Thr1969 in the kinase domain are phosphorylated in ΔN-LRRK2. Given that the kinase activity of LRRK2 is activated by binding of GTP to the ROC domain (*15*, *16*), it would be reasonable to speculate that threonines in the ROC domain are autophosphorylated through interaction with the kinase domain of LRRK2. Interestingly, the peak corresponding to the autophosphorylation of Thr1491 was not observed in the spectra of S1403A and T1410A (Figure 5A). The reason for this discrepancy is not clear, but one possibility would be that the autophosphorylation of Ser1403, Thr1404, and/or Thr1410 is required for the autophosphorylation of Thr1491.

To investigate the functional significance of the autophosphorylation identified in ΔN-LRRK2, we replaced the autophosphorylation sites with alanine or aspartate and found that T1491D mutation causes a significant decrease in the kinase activity as well as the GTP binding activity in cells (Figure 6A,B). Since the GTP binding activity is required for the kinase activity of LRRK2 (*16*), reduction in the GTP-bound form of LRRK2 caused by T1491D mutation might have lowered the kinase activity, implicating the autophosphorylation of the ROC domain in a negative feedback regulation of the kinase activity of LRRK2. We also found that T1967A mutation causes a significant decrease in the kinase activity as well as in the autophosphorylation activity of ΔN- and FL-LRRK2 (Figure 7A,B). In contrast, substitution of Thr1969 located in close proximity to Thr1967 had little effect on its kinase activity (Figure 7A,B), underscoring the importance of Thr1967. Upon substitution of Thr1967 with aspartate to mimic the constitutive phosphorylation of particular threonine residues, T1967D mutant ΔN-LRRK2 showed comparable kinase activity (Figure 7C) to wt, suggesting that phosphorylation on Thr1967 plays a role in maintaining the kinase activity of LRRK2. In contrast, T1967D mutant FL-LRRK2 exhibited a decreased kinase activity (Figure 7D), unlike ΔN-LRRK2. The reason for this discrepancy is yet to be clarified, but one possibility would be that the aspartate substitution failed to effectively mimic the phosphorylation of Thr1967 on holoprotein basis. Substitution of Thr1967 might have caused a subtle distortion in the structure of the kinase domain, as well as an alteration in the functional interactions of the kinase domain with the N-terminal half, within FL-LRRK2, thereby resulting in reduction in the kinase activity by both alanine and aspartate substitutions; it is possible that simplification of the domain structure by deletion of the amino-terminal half of LRRK2 tolerated the T1967D mutation to effectively mimic the phosphorylation status in ΔN-LRRK2. Our finding that the Michaelis constants for ATP of wt or T1967A mutant ΔN-LRRK2 were similar further supports the notion that the kinase domain of T1967A mutant ΔN-LRRK2 is folded in a proper conformation. Moreover, T1967A mutant ΔN- as well as FL-LRRK2 retained the GTP binding activity in cultured cells upon metabolic labeling, too (data not shown). Taken together, we reasoned that the structures of both the ROC and the kinase domains in functional forms are not significantly disrupted by substitution of Thr1967 at least in ΔN-LRRK2.

On the basis of these findings, we generated phosphorylation-specific antibodies against LRRK2 phosphorylated at Thr1967. The antibody recognized in vitro phosphorylated wt ΔN-LRRK2 as well as FL-LRRK2, but not kinase-inactive K1906M mutant (Figure 8B−D). These results indicated that autophosphorylation on Thr1967 occurs in FL-LRRK2 as well as in ΔN-LRRK2. Detection of the kinase activity of LRRK2 has so far depended on in vitro phosphorylation experiments using radioactive reagents. The phospho-specific antibodies described here should serve as useful tools in the facile examination of the kinase activity of LRRK2. In vitro phosphorylation reaction was required to detect the autophosphorylation of LRRK2 by this antibody. This is presumably due to the relatively low sensitivity of the antibody and/or the low extent of autophosphorylation at these residues. Notably, autophosphorylation of G2019S mutant FL-LRRK2 detected by these antibodies was upregulated compared to that of wt FL-LRRK2 (Figure 7C), ensuring the ability of our antibodies to detect an abnormal upregulation of the kinase activity of LRRK2.

In summary, we have identified six autophosphorylation sites in the kinase as well as GTP binding domains in LRRK2, investigated their functional role on the kinase activity and generated an autophosphorylation-specific antibody. Considering that the kinase activity of LRRK2 is abnormally upregulated by FPD mutations (*12*, *13*) and that the cell toxicity of overexpressed FPD mutant LRRK2 depends on its kinase activity (*14*, *15*), elucidation of the regulatory mechanisms of the kinase activity of LRRK2 is vital to the development of novel therapeutic strategies for PD. Given that the LRRK2 is a pro-apoptotic kinase, it is tempting to speculate that the kinase activity of LRRK2 is suppressed at a steady state and upregulated under specific conditions in PARK8 as well as in some form of sporadic PD. In this regard, the autophosphorylation-specific antibody generated in the present study should facilitate the examination of the activation status of LRRK2 under physiological or stress conditions by immunoblotting or in situ, enabling the consequent identification of the upstream events that activate LRRK2. Further elucidation of the regulatory mechanism of LRRK2 as well as identification of its physiologically relevant substrates would lead to a more precise understanding of the role of LRRK2 in the pathomechanism of PD.

ACKNOWLEDGMENT

The authors thank Drs. John Anderson, Zhao Ren, Dale Schenk, and other scientists at Elan Pharmaceuticals, Drs. Hidenori Ichijo, Kohsuke Takeda of the Graduate School of Pharmaceutical Sciences, and current and former lab members for helpful discussions.

SUPPORTING INFORMATION AVAILABLE

Figure S1: MALDI-TOF/MS spectra of ΔN-LRRK2 T1967A and T1969A. Figure S2: Measurement of Michaelis constants of wt and T1967A GST-ΔN-LRRK2 for ATP. This material is available free of charge via the Internet at http://pubs.acs.org.

NOTE ADDED IN PROOF

During the revision stage of this paper, Greggio et al. reported on the identification of autophosphorylation sites within the ROC domain of LRRK2 (*25*), some of which (e.g., Thr1410, Thr1491) correspond to those determined in this present study.

REFERENCES

1. Dawson, T. M., and Dawson, V. L. (2003) Molecular pathways of neurodegeneration in Parkinson's disease. *Science 302*, 819–822.
2. Trojanowski, J. Q., and Lee, V. M. (2003) Parkinson's disease and related alpha-synucleinopathies are brain amyloidoses. *Ann. N.Y. Acad. Sci. 991*, 107–110.
3. Spillantini, M. G., Schmidt, M. L., Lee, V. M., Trojanowski, J. Q., Jakes, R., and Goedert, M. (1997) Alpha-synuclein in Lewy bodies. *Nature 388*, 839–840.
4. Baba, M., Nakajo, S., Tu, P. H., Tomita, T., Nakaya, K., Lee, V. M., Trojanowski, J. Q., and Iwatsubo, T. (1998) Aggregation of alpha-synuclein in Lewy bodies of sporadic Parkinson's disease and dementia with Lewy bodies. *Am. J. Pathol. 152*, 879–884.
5. Moore, D. J., West, A. B., Dawson, V. L., and Dawson, T. M. (2005) Molecular pathophysiology of Parkinson's disease. *Annu. Rev. Neurosci. 28*, 57–87.
6. Paisan-Ruiz, C., Jain, S., Evans, E. W., Gilks, W. P., Simon, J., van der Brug, M., Lopez de Munain, A., Aparicio, S., Gil, A. M., Khan, N., Johnson, J., Martinez, J. R., Nicholl, D., Carrera, I. M., Pena, A. S., de Silva, R., Lees, A., Marti-Masso, J. F., Perez-Tur, J., Wood, N. W., and Singleton, A. B. (2004) Cloning of the gene containing mutations that cause PARK8-linked Parkinson's disease. *Neuron 44*, 595–600.

7. Zimprich, A., Biskup, S., Leitner, P., Lichtner, P., Farrer, M., Lincoln, S., Kachergus, J., Hulihan, M., Uitti, R. J., Calne, D. B., Stoessl, A. J., Pfeiffer, R. F., Patenge, N., Carbajal, I. C., Vieregge, P., Asmus, F., Muller-Myhsok, B., Dickson, D. W., Meitinger, T., Strom, T. M., Wszolek, Z. K., and Gasser, T. (2004) Mutations in LRRK2 cause autosomal-dominant parkinsonism with pleomorphic pathology. *Neuron 44*, 601–607.
8. Healy, D. G., Falchi, M., O'Sullivan, S. S., Bonifati, V., Durr, A., Bressman, S., Brice, A., Aasly, J., Zabetian, C. P., Goldwurm, S., Ferreira, J. J., Tolosa, E., Kay, D. M., Klein, C., Williams, D. R., Marras, C., Lang, A. E., Wszolek, Z. K., Berciano, J., Schapira, A. H., Lynch, T., Bhatia, K. P., Gasser, T., Lees, A. J., and Wood, N. W. (2008) Phenotype, genotype, and worldwide genetic penetrance of LRRK2-associated Parkinson's disease: a case-control study. *Lancet Neurol. 7*, 583–590.
9. Ozelius, L. J., Senthil, G., Saunders-Pullman, R., Ohmann, E., Deligtisch, A., Tagliati, M., Hunt, A. L., Klein, C., Henick, B., Hailpern, S. M., Lipton, R. B., Soto-Valencia, J., Risch, N., and Bressman, S. B. (2006) LRRK2 G2019S as a cause of Parkinson's disease in Ashkenazi Jews. *N. Engl. J. Med. 354*, 424–425.
10. Santpere, G., and Ferrer, I. (2009) LRRK2 and neurodegeneration. *Acta Neuropathol. 117*, 227–246.
11. Bosgraaf, L., and Van Haastert, P. J. (2003) Roc, a Ras/GTPase domain in complex proteins. *Biochim. Biophys. Acta 1643*, 5–10.
12. West, A. B., Moore, D. J., Biskup, S., Bugayenko, A., Smith, W. W., Ross, C. A., Dawson, V. L., and Dawson, T. M. (2005) Parkinson's disease-associated mutations in leucine-rich repeat kinase 2 augment kinase activity. *Proc. Natl. Acad. Sci. U. S. A. 102*, 16842–16847.
13. Gloeckner, C. J., Kinkl, N., Schumacher, A., Braun, R. J., O'Neill, E., Meitinger, T., Kolch, W., Prokisch, H., and Ueffing, M. (2006) The Parkinson disease causing LRRK2 mutation I2020T is associated with increased kinase activity. *Hum. Mol. Genet. 15*, 223–232.
14. Greggio, E., Jain, S., Kingsbury, A., Bandopadhyay, R., Lewis, P., Kaganovich, A., van der Brug, M. P., Beilina, A., Blackinton, J., Thomas, K. J., Ahmad, R., Miller, D. W., Kesavapany, S., Singleton, A., Lees, A., Harvey, R. J., Harvey, K., and Cookson, M. R. (2006) Kinase activity is required for the toxic effects of mutant LRRK2/dardarin. *Neurobiol. Dis. 23*, 329–341.
15. Smith, W. W., Pei, Z., Jiang, H., Dawson, V. L., Dawson, T. M., and Ross, C. A. (2006) Kinase activity of mutant LRRK2 mediates neuronal toxicity. *Nat. Neurosci. 9*, 1231–1233.
16. Ito, G., Okai, T., Fujino, G., Takeda, K., Ichijo, H., Katada, T., and Iwatsubo, T. (2007) GTP binding is essential to the protein kinase activity of LRRK2, a causative gene product for familial Parkinson's disease. *Biochemistry 46*, 1380–1388.
17. Greggio, E., Zambrano, I., Kaganovich, A., Beilina, A., Taymans, J. M., Daniels, V., Lewis, P., Jain, S., Ding, J., Syed, A., Thomas, K. J., Baekelandt, V., and Cookson, M. R. (2008) The Parkinson disease-associated leucine-rich repeat kinase 2 (LRRK2) is a dimer that undergoes intramolecular autophosphorylation. *J. Biol. Chem. 283*, 16906–16914.
18. Miller, S. G., and Kennedy, M. B. (1986) Regulation of brain type II Ca2+/calmodulin-dependent protein kinase by autophosphorylation: a Ca2+-triggered molecular switch. *Cell 44*, 861–870.
19. Li, X., Lu, Y., Jin, W., Liang, K., Mills, G. B., and Fan, Z. (2006) Autophosphorylation of Akt at threonine 72 and serine 246. A potential mechanism of regulation of Akt kinase activity. *J. Biol. Chem. 281*, 13837–13843.
20. Noble, C., Mercer, K., Hussain, J., Carragher, L., Giblett, S., Hayward, R., Patterson, C., Marais, R., and Pritchard, C. A. (2008) CRAF autophosphorylation of serine 621 is required to prevent its proteasome-mediated degradation. *Mol. Cell 31*, 862–872.
21. Tomita, T., Maruyama, K., Saido, T. C., Kume, H., Shinozaki, K., Tokuhiro, S., Capell, A., Walter, J., Grunberg, J., Haass, C., Iwatsubo, T., and Obata, K. (1997) The presenilin 2 mutation (N141I) linked to familial Alzheimer disease (Volga German families) increases the secretion of amyloid beta protein ending at the 42nd (or 43rd) residue. *Proc. Natl. Acad. Sci. U. S. A. 94*, 2025–2030.
22. West, A. B., Moore, D. J., Choi, C., Andrabi, S. A., Li, X., Dikeman, D., Biskup, S., Zhang, Z., Lim, K. L., Dawson, V. L., and Dawson, T. M. (2007) Parkinson's disease-associated mutations in LRRK2 link enhanced GTP-binding and kinase activities to neuronal toxicity. *Hum. Mol. Genet. 16*, 223–232.
23. Jaleel, M., Nichols, R. J., Deak, M., Campbell, D. G., Gillardon, F., Knebel, A., and Alessi, D. R. (2007) LRRK2 phosphorylates moesin at threonine-558: characterization of how Parkinson's disease mutants affect kinase activity. *Biochem. J. 405*, 307–317.
24. Österberg, R. (1957) Metal and hydrogen-ion binding properties of o-phosphoserine. *Nature 179*, 476–477.
25. Greggio, E., Taymans, J. M., Zhen, E. Y., Ryder, J., Vancraenenbroeck, R., Beilina, A., Sun, P., Deng, J., Jaffe, H., Baekelandt, V., Merchant, K., and Cookson, M. R. (2009) The Parkinson's disease kinase LRRK2 autophosphorylates its GTPase domain at multiple sites. *Biochem. Biophys. Res. Commun. 389*, 449–454.